Equivalence of four Monte Carlo methods for photon migration in turbid media

Angelo Sassaroli[1,*] and Fabrizio Martelli[2]

[1]*Tufts University, Department of Biomedical Engineering, 4 Colby Street, Medford, Massachusetts 02155, USA*
[2]*Dipartimento di Fisica e Astronomia dell'Università degli Studi di Firenze, Via G. Sansone 1, Sesto Fiorentino, Florence 1-50019, Italy*
**Corresponding author: angelo.sassaroli@tufts.edu*

Received July 6, 2012; accepted August 13, 2012;
posted August 23, 2012 (Doc. ID 172118); published September 13, 2012

In the field of photon migration in turbid media, different Monte Carlo methods are usually employed to solve the radiative transfer equation. We consider four different Monte Carlo methods, widely used in the field of tissue optics, that are based on four different ways to build photons' trajectories. We provide both theoretical arguments and numerical results showing the statistical equivalence of the four methods. In the numerical results we compare the temporal point spread functions calculated by the four methods for a wide range of the optical properties in the slab and semi-infinite medium geometry. The convergence of the methods is also briefly discussed. © 2012 Optical Society of America

OCIS codes: 170.3660, 170.5280, 290.7050, 300.1030.

1. INTRODUCTION

There are no general analytical methods to solve the radiative transfer equation (RTE); therefore, one has to resort to some numerical methods. Among the numerical methods, one that stands out in terms of flexibility for modeling the geometry of the medium and the distribution of the optical properties is the Monte Carlo (MC) method. MC methods have been used in many fields of research and also largely in tissue optics [1–5], both in diffusive regimes (e.g., breast imaging [6] and functional brain imaging [7,8]) and nondiffusive regimes (confocal microscopy [9] and optical coherence tomography [10]). Other MC applications include photodynamic therapy [11], laser doppler [12], and pulse oximetry [13].

For applications in tissue optics, it would be extremely important to rely on "numerical phantoms," that is, a collection of numerical data that are considered a reference for transport calculations. An example of such a numerical phantom can be found in the data presented in [14]. A numerical phantom can be used for several purposes: (a) for validating approximate models of photon migration (e.g., in diffusion conditions), (b) as reference data for validating retrieval algorithms for the inverse problem, and (c) as a guideline in experimental investigations. In practice, in the same way as an optical phantom is used to evaluate the performance of near-IR instrumentation, a numerical phantom could play a similar role for validating the performance of forward and inverse solvers. However, a numerical phantom widely accepted for all the applications in tissue optics is still missing. The reason for this lies in the lack of standardization and cross validation among the MC codes developed for biomedical applications. Currently several MC methods based on different rules of path length extraction are available in the field of tissue optics. These rules are widely accepted because they are obtained from fundamental properties of photon interaction in turbid media. At the same time, questions have been raised recently about the equivalence and convergence of these methods that are based on different rules of path length extraction, especially when diffusion conditions are not fulfilled [15–17]. In this work, we address this question by comparing the results given by four widely used MC methods. We provide numerical results for a wide range of situations, including those in nondiffusive regimes. The results show that all the MC methods converge to the same values and that the discrepancies found are only due to the limited statistics. These results are substantiated by theoretical arguments showing the statistical equivalence of the four MC methods.

Briefly, we want to review the key rules of MC methods. At the core of every MC method there is a pseudorandom number generator, where the random numbers are uniformly distributed in the interval (0,1). The key point for MC simulations is the generation of the trajectories, which is done by using the same statistical rules that govern propagation in random media. A photon path is built as a sequence of straight line segments, starting at the source location and ending either outside the medium (lost photon) or inside the detector (useful photon). Each segment is calculated by extracting three random numbers w_1, w_2, w_3. The first two numbers w_1, w_2 are associated with the angles θ_i and ϕ_i [the angles identify the direction of propagation $\hat{s}_i \equiv (\theta_i, \phi_i)$]; a third random number w_3 is associated with the pathlength l_i along the direction $\hat{s}_i$. A fourth random number is extracted when a photon reaches the boundary of the medium in order to determine whether reflection or transmission occurs. The rules used to associate random numbers with the trajectory's segments originate from the properties of RTE, and thus from the basic statistical rules of absorption and scattering interactions.

In Section 2, after introducing the RTE, we describe four MC methods that are characterized by different statistical rules of path length extraction and weight factor assignment. The four MC methods share the same statistical rules for the

 © 2012 Optical Society of America

calculation of the direction of propagation after a scattering event has occurred. We will not describe how reflections at the boundaries of the medium are calculated in detail, since we will assume that the same rules are used by the four methods. We will refer to these methods as the "albedo-weight" method (AW) [2], the "albedo-rejection" method (AR) [18], the "absorption-scattering path length rejection" method (ASPR) [11,16,17], and the microscopic Beer–Lambert law method (mBLL) [14,15]. The four methods reduce to the same one for the case of a nonabsorbing medium. The equivalence of the four methods is obtained by studying the *a priori* probability of occurrence of a detected trajectory and its corresponding weight in a general situation. In Section 3, we compare the temporal point spread functions (TPSFs), generated by the four methods, in situations where diffusion conditions are not fulfilled. In Section 4, we briefly discuss the different speeds of convergence together with other features of the four methods.

2. THEORY

A. Solution of RTE for Ballistic Radiation

The propagation of photons in a random medium is described by the RTE:

$$\frac{1}{v}\frac{\partial I(\mathbf{r},\hat{s},t)}{\partial t}+\hat{s}\cdot\nabla I(\mathbf{r},\hat{s},t)+[\mu_a(\mathbf{r})+\mu_s(\mathbf{r})]I(\mathbf{r},\hat{s},t)=\mu_s(\mathbf{r})\int_{4\pi}p(\hat{s}\cdot\hat{s}')I(\mathbf{r},\hat{s}',t)\mathrm{d}\omega'+S(\mathbf{r},\hat{s},t). \quad (1)$$

In Eq. (1) I is the specific intensity (or radiance; $[I]=L^{-2}t^{-1}$) where $\mathbf{r}$, $\hat{s}$, and t are the spatial, angular, and temporal variables, respectively, $p(\hat{s}\cdot\hat{s}')$ is the phase function, S is a source term, $d\omega'$ is the infinitesimal solid angle around the direction $\hat{s}'$, and v is the speed of light in the medium. μ_s and μ_a are the scattering and the absorption coefficients, respectively, and $\mu_t=\mu_a+\mu_s$ is the extinction coefficient. The Green function of Eq. (1) is obtained when the source term is defined as $S(\mathbf{r},\hat{s},t)=\delta(\mathbf{r})\delta(\hat{s}-\hat{s}_0)\delta(t)$. Equation (1) originates from general principles of particle/energy balance (principle of conservation of energy) inside an infinitesimal volume of the medium. Classically, a photon traveling in a random medium (having constant v, or region-wise constant v) traces a trajectory that is a sequence of straight-line segments changing orientation after each scattering event according to the phase function of the medium (Fig. 1). In order to introduce the rules for path length extraction in the four different MC methods, we need to write the solution of RTE for the ballistic radiance, which reflects the extinction properties of radiation. The RTE for the ballistic radiance reduces to the following equation:

$$\frac{1}{v}\frac{\partial I(\mathbf{r},\hat{s},t)}{\partial t}+\hat{s}\cdot\nabla I(\mathbf{r},\hat{s},t)+\mu_t(\mathbf{r})I(\mathbf{r},\hat{s},t)=\delta(\mathbf{r})\delta(\hat{s}-\hat{s}_0)\delta(t). \quad (2)$$

The solution of Eq. (2) is

$$I(\mathbf{r},\hat{s},t)=v\delta(|\mathbf{r}|-vt)\delta(\hat{s}-\hat{s}_0)\exp\left(-\int_0^l\mu_t(\xi)\mathrm{d}\xi\right), \quad (3)$$

where $\mathbf{r}=l\hat{s}_0$. Equation (3) gives us the attenuation of power along the "ray" determined by the initial direction of propagation $\hat{s}_0$. The exponential in Eq. (3) is interpreted as the cumulative probability of a photon free flight in $(0,\ l)$ (i.e., absence of an extinction event), and therefore it can be associated with a unique random number w uniformly distributed in (0,1). In other words, by extracting w we can always define a unique free path length l. In the next four subsections we will describe the four MC methods.

B. Albedo-Weight Method

In this method the free path length traveled by the photon between two consecutive extinction events is associated with a random number w by the rule described above:

$$w=\exp\left(-\int_0^l\mu_t(\xi)\mathrm{d}\xi\right). \quad (4)$$

It is not generally possible to analytically invert Eq. (4) (but it is always possible numerically); however, we can easily derive the distribution of probability density for the free path length "l":

$$p(l)=\mu_t(l)\exp\left(-\int_0^l\mu_t(\xi)\mathrm{d}\xi\right). \quad (5)$$

More precisely, $p(l)$ represents the probability density of having an extinction event at "l" when the photon started at $l=0$ (along $\hat{s}_0$). Note that $p(l)$ is correctly normalized to "1" over the range of path lengths $(0,\infty)$. For example, if μ_t is constant along direction $\hat{s}_0$, Eq. (4) can be easily inverted, and we obtain

$$\frac{-\ln(w)}{\mu_t}=l. \quad (6)$$

The probability of having an extinction event at l (along $\hat{s}_0$) is larger than the probability of having a scattering event at l; therefore, in order to propagate the traveling photon to the next direction, a weight factor is assigned to the photon at the interaction point. The weight factor is the albedo $a(\hat{s}_0,l)$ calculated along $\hat{s}_0$ at a distance "l" from the starting point $(l=0):a(\hat{s}_0,l)=\mu_s(\hat{s}_0,l)/\mu_t(\hat{s}_0,l)$. After an interaction event has occurred, we extract the new direction of propagation $\hat{s}_1\equiv(\theta_1,\phi_1)$ according to the phase function of the medium. After repeating these steps many times, the photon can be lost or detected. In the latter case a weight factor $[W(\Gamma)]$ is assigned to the whole trajectory (Γ):

$$W(\Gamma)=\prod_{\Gamma}a(\hat{s}_i,l_i). \quad (7)$$

The term on the right in Eq. (7) is the product of the albedos at the vertices of the trajectory Γ, which is defined by the sequence $(\hat{s}_0,l_0),(\hat{s}_1,l_1),\ldots(\hat{s}_{n-1},l_{n-1})$, where we have assumed that the photon has been detected after "n" scattering events [Fig. (1)]. Each couple $(\hat{s}_i,l_i)$ describes the path length "l_i" spent along the direction $\hat{s}_i$. Note that if we change the distribution of either the scattering or the absorption coefficient (or both), different trajectories (with different weights) will be favored by detected photons. In the following formulas we will consider the variable $\hat{s}_i$ as implicit in the arguments of the albedos and in those of the optical properties. In order to dispel a possible source of confusion, note that the optical properties depend only on the point of observation inside the medium

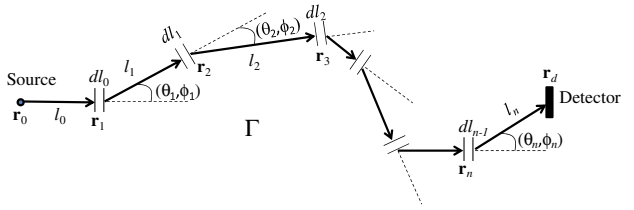

Fig. 1. (Color online) Trajectory Γ is shown. Each direction $\hat{s}_i$ is defined by the couple of angles (θ_i, ϕ_i) $(i = 1, 2 \ldots n)$, but the phase function is assumed to depend on the angle θ_i only. The interactions occur within the spatial intervals dl_{i-1} centered at $\mathbf{r}_i$ $(i = 1, 2 \ldots n)$ and to within the solid angles $d\omega_i$ (not shown) surrounding the directions $\hat{s}_i$.

(and not on the direction of observation). The directions $\hat{s}_i$ in the arguments of the albedos were used only to describe the directions of the segments along a trajectory.

C. Albedo-Rejection Method

In this method we use the same rule of path length extraction (l) as before, i.e., according to the inversion of Eq. (4). Afterward we extract another random number "w" uniformly distributed in (0,1) and propagate or terminate the trajectory according to whether $w \le a(l)$ or $w > a(l)$, respectively ([18], p. 535). Since w is uniformly distributed in (0, 1), the probability that $w \le a(l)$ is $a(l)$. In this method the weight applied to the trajectory Γ is

$$W(\Gamma) = 1. \tag{8}$$

We note that also for this method the trajectories favored by detected photons are dependent on the distribution of both the scattering and absorption coefficients of the medium.

D. Microscopic Beer–Lambert Law Method

We rewrite Eq. (3) as

$$I(\mathbf{r}, \hat{s}, t) = v\delta(|\mathbf{r}| - vt)\delta(\hat{s} - \hat{s}_0) \exp\left(-\int_0^l \mu_s(\xi)\mathrm{d}\xi\right) \times \exp\left(-\int_0^l \mu_a(\xi)\mathrm{d}\xi\right). \tag{9}$$

Equation (9) suggests that we can study the problem of photon migration by first considering the nonabsorbing medium and afterward applying the weight factor:

$$W(\Gamma) = \exp\left(-\int_\Gamma \mu_a(\xi)\mathrm{d}\xi\right), \tag{10}$$

where the integral is calculated along the whole trajectory. The path length extraction in this method uses Eq. (4) that is rewritten by using μ_s instead of μ_t. This implies that (a) regardless of the distribution of the absorption coefficient of the medium, detected photons will choose the same trajectories, and (b) the weight factor assigned to those trajectories changes according to Eq. (10). These two statements constitute the so-called microscopic Beer–Lambert law.

E. Absorption-Scattering Path Length Rejection Method

In this case we extract two random numbers uniformly distributed in (0, 1), w_1 and w_2, and we define them as

$$w_1 = \exp\left(-\int_0^{ls} \mu_s(\xi)\mathrm{d}\xi\right),$$
$$w_2 = \exp\left(-\int_0^{la} \mu_a(\xi)\mathrm{d}\xi\right). \tag{11}$$

After inverting Eq. (11), one compares l_s with l_a (for homogeneous medium $l_s = -ln(w_1)//\mu_s$, $l_a = -ln(w_2)//\mu_a$) and propagates or terminates the photon according to whether $l_s \le l_a$ or $l_s > l_a$, respectively. When the trajectory is detected, the weight factor applied is

$$W(\Gamma) = 1. \tag{12}$$

Also for this method, as for AW and AR methods, the actual trajectories chosen by detected photons are dependent on the distribution of both the scattering and absorption coefficients of the medium.

F. Equivalence of the Four MC Methods

In the following sections (Subsections 2.F.1 throudh 2.F.5) we will provide some arguments that show the statistical equivalence of the four MC methods. Let's consider an arbitrary detected trajectory Γ (Fig. 1) and calculate both the infinitesimal probability of its occurrence and its weight according to the rules defined for the four MC methods. Finally, we define the weighted probability to detect a photon that has traveled along Γ as the product of the probability to follow the given trajectory and the weight assigned to that trajectory. We will not address the difficult issue of "probability normalization" over the nonnumerable space of all possible trajectories, assuming that it is always possible to define it. The probability of the occurrence of a trajectory from the statistical viewpoint coincides with the probability of extracting a particular sequence of random numbers w_i, from which the path lengths (l_i) and the directions ($\hat{s}_i$) of the trajectory are calculated, and also the rejection criteria (for the AR and ASPR methods) are overcome. We observe that the independence of the random variables w_i implies the independence of the random variables l_i, θ_i, and ϕ_i, which are derived from w_i. Therefore, the conjunct probability density of a set of random variables is given by the product of the probability density of each random variable of the set. Since all the MC methods share the same rule for the calculation of $\hat{s}_i$, we will not detail how the angles (θ_i, ϕ_i) are calculated from a couple of random numbers (w_{i1}, w_{i2}). We will simply assume that the probability of extracting a direction $\hat{s}_i$ within a solid angle $d\omega_i$ is given by $P(\hat{s}_i, d\omega_i) = p(\theta_i)d\omega_i$, where $p(\theta_i)$ is the phase function of the medium along the scattering angle θ_i.

1. AW Method

By the AW method the infinitesimal probability of having an interaction in the interval $(l_i, l_i + dl_i)$ is

$$dP(l_i, l_i + dl_i) = \mu_t(l_i)dl_i \exp\left(-\int_0^{l_i} \mu_t(\xi)\mathrm{d}\xi\right). \tag{13}$$

Because of the aforementioned independence of the random variables l_i and θ_i, it is straightforward to assign to the trajectory Γ the probability of its occurrence, $dP(\Gamma)$ (see Fig. 1):

$$dP(\Gamma) = \left[\prod_{i=0}^{n-1} \mu_t(l_i) dl_i p(\theta_{i+1}) d\omega_{i+1}\right] \times \exp\left(-\int_\Gamma \mu_t(\xi) d\xi\right). \quad (14)$$

The weight assigned to the trajectory is

$$W(\Gamma) = \prod_{i=0}^{n-1} a(l_i). \quad (15)$$

In Eqs. (14) and (15), n is the number of interaction events inside the medium.

2. AR Method

In the AR method each path length l_i is extracted with the same rule as in the AW method; however, an additional random variable w is extracted and compared with $a(l_i)$. Therefore, we have to consider the conjunct probability of having an interaction at $(l_i, l_i + dl_i)$ and having $w < a(l_i)$. This conjunct probability is given by

$$dP\{[l_i, w] \in [l_i, l_i + dl_i] \times [0, a(l_i)]\} = a(l_i)\mu_t(l_i) dl_i \exp\left(-\int_0^{l_i} \mu_t(\xi) d\xi\right). \quad (16)$$

Because of the independence of all the random variables, we can write the expression of the probability of occurrence of Γ as

$$dP(\Gamma) = \left[\prod_{i=0}^{n-1} a(l_i)\mu_t(l_i) dl_i p(\theta_{i+1}) d\omega_{i+1}\right] \times \exp\left(-\int_\Gamma \mu_t(\xi) d\xi\right). \quad (17)$$

The weight of the trajectory is

$$W(\Gamma) = 1. \quad (18)$$

Note that the AR and AW methods are immediately "comparable": given an arbitrary trajectory, the probability of its occurrence according to the AR method is always lower than that of the AW method, while the opposite is true for the weight.

3. mBLL Method

By the mBLL method, the probability of having an interaction in the interval $(l_i, l_i + dl_i)$ is

$$dP(l_i, l_i + dl_i) = \mu_s(l_i) dl_i \exp\left(-\int_0^{l_i} \mu_s(\xi) d\xi\right). \quad (19)$$

The probability associated with the trajectory Γ is

$$dP(\Gamma) = \left[\prod_{i=0}^{n-1} \mu_s(l_i) dl_i p(\theta_{i+1}) d\omega_{i+1}\right] \times \exp\left(-\int_\Gamma \mu_s(\xi) d\xi\right), \quad (20)$$

while the weight assigned to it is

$$W(\Gamma) = \exp\left(-\int_\Gamma \mu_a(\xi) d\xi\right). \quad (21)$$

Also, for the mBLL method the probability $dP(\Gamma)$ is always larger than that of the AR method, while the opposite is true for $W(\Gamma)$. Note also that the mBLL and AW methods are not "comparable" in general, since the relationships between the probability of the occurrence of a trajectory Γ and the weight are dependent on the particular trajectory considered. For example, if we consider a homogeneous medium, the lengths of a section l_i favored by the AW and mBLL methods are on average equal to $1/\mu_t$ and $1/\mu_s$, respectively.

4. ASPR Method

According to this method, the probability of an interaction occurring at $(l_i, l_i + dl_i)$ coincides with the conjunct probability that the couple of random variables extracted, l_s and l_a, are found in the region $(l_i, l_i + dl_i) \times (l_i, \infty)$. This probability corresponds to (the details are given in Appendix A)

$$dP\{[l_s, l_a] \in [l_i, l_i + dl_i] \times [l_i, \infty]\} = \mu_s(l_i) dl_i \times \exp\left(-\int_0^{l_i} \mu_s(\xi) d\xi\right) \exp\left(-\int_0^{l_i} \mu_a(\xi) d\xi\right). \quad (22)$$

The probability associated with the trajectory Γ is coincident with Eq. (17), which was obtained for the AR method. The same is true for the weight factor, which is given by Eq. (18). Therefore, the AR and ASPR methods are characterized by the same weight and also by similar trajectories, having on average the same segments' lengths.

5. Comparison among the Methods

By looking at the expressions of $dP(\Gamma)$ and $W(\Gamma)$ in the four methods, we conclude that the weighted probability for a photon to be detected after tracing an arbitrary trajectory Γ, which is given by $dP(\Gamma)W(\Gamma)$, is independent of the method used. As a consequence, the total probability of detecting a photon [continuous wave case (CW)], or the probability of detecting a photon in a short time interval [time domain case (TD)], is also equivalent in the four MC methods. The definition of the probability of detecting a photon in CW is

$$P = \int_{S(\Gamma)} dP(\Gamma) W(\Gamma), \quad (23)$$

where the integral is carried out over the space of all the possible trajectories $[S(\Gamma)]$ that connect the source and detector. The definition of TPSF in a time interval $(t_i, t_i + dt)$ is

$$\mathrm{TPSF}(t_i, t_i + dt) = \int_{S[\Gamma(t_i, t_i + dt)]} dP(\Gamma) W(\Gamma), \quad (24)$$

where the integral is carried out over the subspace of all the possible trajectories that connect the source and detector having a total time of flight in the interval $(t_i, t_i + dt)$.

Now let's rewrite Eq. (24) for an actual MC simulation. Assume that N and n_i are the number of injected photons and the number of photons detected in the time interval $(t_i, t_i + dt)$, respectively. Each detected trajectory characterized by an arrival time in the interval $(t_i, t_i + dt)$ will be unique, and its *a posteriori* probability (or frequency) is $dP(\Gamma) = 1/N$, while its weight depends on the method used. Therefore, we can rewrite Eq. (24) for the actual TPSF as

$$\mathrm{TPSF}(t_i, t_i + dt) = \frac{n_i}{N}\langle W(\Gamma)\rangle. \quad (25)$$

In Eq. (25) the average value is calculated by using all the n_i detected trajectories having a total time of flight in the interval considered. Note that for a general distribution of the optical properties, the random variables of Eq. (25) are both n_i and $W(\Gamma)$ for the AW and mBLL methods, and only n_i for the AR and ASPR methods. For homogeneous media the random variables in Eq. (25) reduce to n_i alone for the mBLL method also. In the next section the TPSFs defined by Eq. (25) have been divided by the temporal range "dt" and the detector's area "ΔS."

3. RESULTS

We compared the results of independent MC simulations carried out using the four independent MC methods. The four methods have been inserted on the same MC code by only changing the rules of trajectories' extraction according to the definitions given above. We have covered a wide range of situations for the slab and the semi-infinite medium. All the figures described in this section refer to the reflectance from a slab 1 mm thick, with $\mu_a = \mu_s = 1\ \mathrm{mm}^{-1}$. The Henyey–Greenstein phase function with asymmetry factor $g = 0$ has been considered. The refractive indices of the medium and the surroundings are 1.4 (no mismatch). The MC simulations were carried out for 100 different source–detector distances in the range 0.079–21.58 mm, and a total number of 10^9 photons were launched. The total number of detected photons ranged from about $1.13\,10^8$ (ASPR) to $3.41\,10^8$ (mBLL).

In Fig. 2 we compare the time-resolved reflectance calculated according to the four methods at source–detector distances of $\rho = 0.079$ mm (left panel) and $\rho = 0.429$ mm (right panel). From this figure the difference in the convergence of the methods can be appreciated: the AR and ASPR methods show a scarcity/absence of detected photons at late arrival times; on the contrary, the AW and mBLL methods show good convergence at late arrival times. This behavior is especially visible at $\rho = 0.429$ mm, where no photon is detected by the AR and ASPR methods after ~25 ps. We can also see that the AW method is characterized by a wider variance than the mBBL method. This result is expected, at least for homogeneous media, since the TPSF in a certain temporal range according to the AW method depends upon two random variables: the number of detected photons and the weight of each detected photon in that range [Eq. (25)]. On the contrary, for the mBLL method the calculation of the TPSF depends only upon the number of photons received in the temporal range considered.

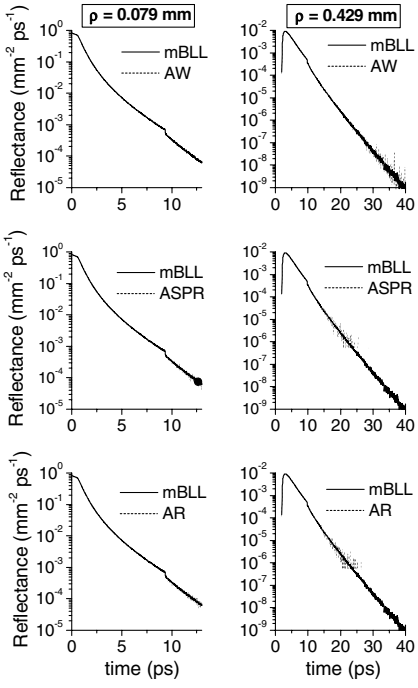

Fig. 2. Time-resolved reflectance from a slab 1 mm thick at the distances 0.079 mm (left panel) and 0.429 mm (right panel) from the input source. The optical properties of the medium are $\mu_a = 1\ \mathrm{mm}^{-1}$, $\mu_s' = 1\ \mathrm{mm}^{-1}$; the refractive index of the medium and the surroundings is 1.4. The Henyey–Greenstein phase function with asymmetry factor $g = 0$ is used.

In Fig. 3 we plot the ratios of the time-resolved reflectance obtained with the AW, ASPR, and AR methods to the reflectance obtained with the mBLL method for the distances 0.079 mm (left panel) and 0.429 mm (right panel). Although the error bars on the data are not shown (since they would not be visible on the plots), the oscillations of the ratios around 1 indicate the statistical equivalence of the methods.

In Fig. 4 we show the ratio of the CW reflectance obtained with the AW, ASPR, and AR methods to the reflectance obtained with the mBLL method, i.e., $R_{\mathrm{AW}}/R_{\mathrm{mBLL}}$, $R_{\mathrm{AR}}/R_{\mathrm{mBLL}}$, and $R_{\mathrm{ASPR}}/R_{\mathrm{mBLL}}$, for a range of distances from 0.079 to 2.5 mm. We did not consider the ratios for distances larger than 2.5 mm, because the CW calculated by the AR and ASPR methods (due to the scarcity of detected photons) were affected by relatively large errors. The slower convergence of the AR and ASPR methods given a fixed number of injected photons is a consequence of the photons' termination used by

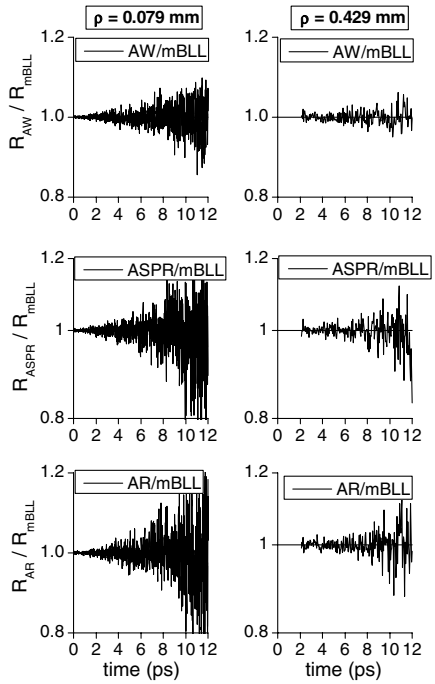

Fig. 3. Same as Fig. 2, except for the ratios of the time-resolved reflectance obtained with the AW, ASPR, and AR methods to the reflectance obtained with the mBLL method.

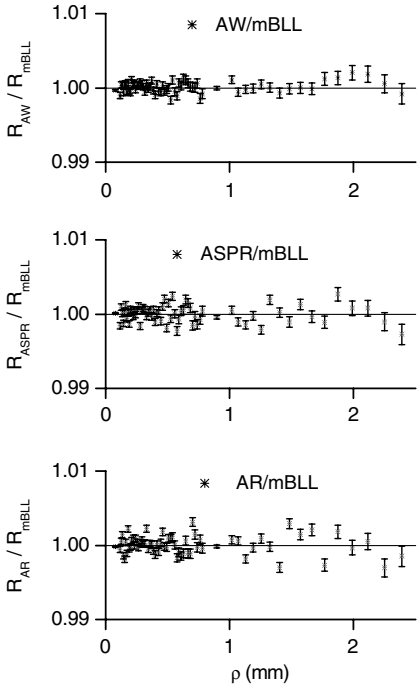

Fig. 4. Same as Fig. 2, except for the ratios between the CW reflectance obtained with the AW, ASPR, and AR methods to the reflectance obtained with the mBLL method, plotted versus the source–detector distance. The error bars represent the standard deviation of the ratios.

these methods. The convergence of these two methods becomes slower and slower as we increase the source–detector separation. The error bars represent the standard deviations of the ratios, which were obtained by error propagation of the standard deviations of the MC results. The standard deviations of the MC simulations were obtained by using the results of 10 independent simulations. For most of the distances shown in Fig. 4, the agreement is within one standard deviation, while especially for the larger distances, due to the lower number of received photons for the AR and ASPR methods, the agreement is within about three standard deviations.

In Fig. 5 we compared the temporal convergence of the ASPR and mBLL methods by carrying out two simulations with the same computation time (2 min) during which 100,500,000 and 144,000,000 photons were launched for the mBLL and the ASPR simulations, respectively. The geometrical and optical properties of the medium were the same as those considered in the previous figures, and the results refer to the distances of 1.02 mm (left panel) and 3.28 mm (right panel). The figure shows a comparison of the time-resolved reflectance (top panels) and the time-resolved ratio of the standard deviations (bottom panel) calculated with the two methods. The standard deviation in each temporal range was calculated by repeating 10 independent simulations. The figure shows that a lower standard deviation is obtained with the mBLL at any time, a result that emphasizes better convergence of this method (higher speed in detecting photons). In general, the convergence performance of the different MC methods depends on several factors, such as the geometrical and optical properties of the medium and the asymmetry parameter. Therefore, we cannot generalize the results obtained for this geometry and this set of optical properties. For example, in the semi-infinite medium geometry for $\mu_a = 0.01$ mm^{-1},

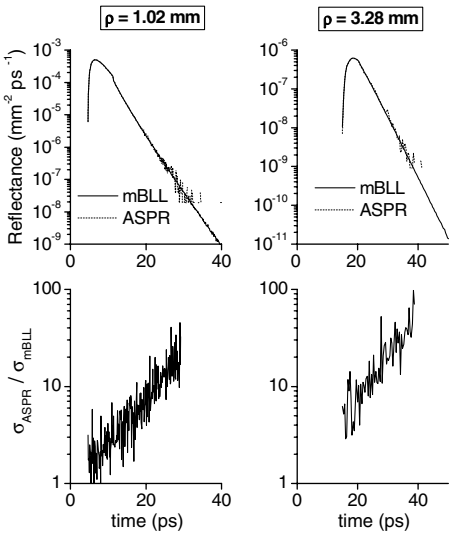

Fig. 5. Comparison between the time-resolved reflectances obtained with the mBLL and ASPR methods. The ratio of the standard deviation obtained with the ASPR method to the standard deviation obtained with the mBLL method is also plotted. The figure pertains to the same slab as the previous figures, and the source–detector distances are 1.02 mm (left panel) and 3.28 mm (right panel).

$\mu_s = 1$ mm^{-1}, and isotropic scattering, we have found that the convergence of the ASPR (and AR) method is faster than that of the mBLL method up to a distance of about 20 mm.

Similar comparisons between the four MC methods were obtained for transmittance through the same slab and for the reflectance from a semi-infinite medium with the same optical properties as the slab. Moreover, similar results to those shown in Figs. 3 and 4 were obtained using the Henyey–Greenstein phase function with $g = 0.8$, refractive indices of the external and internal media of 1 and 1.4, respectively, and optical properties $\mu_s = 5$ mm^{-1}, $\mu_a = 1$ mm^{-1}. We also carried out a simulation in the semi-infinite medium geometry at a source–detector distance of 0.15 mm, with isotropic scattering, and with absorption and scattering coefficients of $\mu_a = 4.5$ mm^{-1}, $\mu_s = 3$ mm^{-1}, respectively. In all the situations investigated we have not found any discrepancy between the MC methods that could not be explained by the limited statistics used in the simulations.

4. DISCUSSION AND CONCLUSION

In this work, we have addressed from a theoretical and numerical point of view the issue of the equivalence of four widely used MC methods that are characterized by different choices of path length extraction. The equivalence of the four MC methods was derived by considering the space of all the possible trajectories connecting the source and detector (useful trajectories). In an actual MC simulation we collect a sample of trajectories that is a numerable subspace of the whole space of useful trajectories. In the four MC methods considered in this work, detected photons follow different trajectories, associated with different weights. Note, for example, that in a homogeneous medium the mean free path length between two interaction events (i.e., the average length of each segment) is $1/\mu_t$ (AW, AR, ASPR) and $1/\mu_s$ (mBLL). In other words, with the exception of only the mBLL method, the trajectories depend on the distribution of both optical

properties. This different characteristic of the four MC methods prompts a question about their convergence performance. In the Section 3 we have briefly addressed this issue by considering two viewpoints: (a) how many photons we should inject in the medium in order to obtain a given accuracy of the TPSF and (b) how much computation time is needed in order to obtain a given accuracy of the TPSF. The convergence of an MC method based on the number of launched photons shows that AW and mBLL are superior to AR and ASPR in a general situation. In fact, in the mBLL and AW methods the photons are not terminated unless they are lost or detected. Therefore, a larger number of photons are detected by the AW and mBLL methods for a given number of launched photons. As for the convergence of a method based on the computation time, we have found that in most of the situations investigated mBLL is superior to the other MC methods, especially when diffusion conditions are not fulfilled. For values of the absorption and scattering coefficients typical of tissue in the near-IR range, the AR and ASPR methods can show faster convergence, at least for "short" source–detector separations (up to about 20 mm in the situations investigated). We also note that the convergence performance of the AR and ASPR methods are the same regardless of whether we are considering the number of injected photons or the computation time. We can say that the AR and ASPR methods are equivalent under any viewpoint one can consider. In contrast, the convergence performance (from both viewpoints) of the AW method is slightly lower than that of the mBLL method in all the situations considered. Last, we recall that the convergence of a TPSF is easily defined based on the number of detected photons: for the AR and ASPR methods (also for the mBLL method for homogeneous media), an estimate of the accuracy of the calculated TPSF in a given temporal range is $1/\sqrt{n_i}$, where n_i is the number of detected photons in the temporal range. This well known property of the binomial distribution, together with the convergence discussed in Subsection 2.F.5, gives us an indication of how "close" we should expect the TPSFs calculated by different methods in a given temporal range to be.

In this paragraph we want to discuss other properties of the four MC methods that, in our opinion, indicate a greater flexibility of the AW and mBLL methods. The four MC methods can be divided into those with weight factor "1" (AR, ASPR) and those with weight factor W different from "1" (AW, mBLL). In the AR and ASPR methods the photon is detected or lost similarly to what happens in a time-resolved experiment in which photons are detected using the time-correlated single-photon counting technique. The noise on the simulated response reproduces the Poisson statistics that typically characterize the noise in experiments. Therefore, in principle the AR and ASPR methods reproduce a more physical simulation of propagation than the AW and mBLL methods. In the AW and mBLL methods simulated "photons" represent energy packets rather than physical photons. However, we note that we can reproduce a more realistic simulation of photon propagation even with the AW and mBLL methods. If we are interested in reproducing the signal (and the noise) detected in an actual experiment, the photons can be terminated afterward, once the simulation is run. We just need to store the weight (W) assigned to each detected photon (by either the mBLL or AW method) and compare it with a random number (w); we terminate a photon if $w > W$, and otherwise (if $w < W$) the photon survives with weight "1". Therefore, by the AW and mBLL methods we obtain more information than by using the AR and ASPR methods. In our opinion the advantages of the AR and ASPR methods are restricted to a range of situations where they can converge faster than the AW and mBLL methods.

In conclusion, the results obtained in Figs. 2–5 confirm the statistical equivalence of the four different MC methods. In general, for the validation of an MC simulator, it would be very useful to compare the results of simulations with those obtained from exact theories. Unfortunately, there are very few examples of analytical solutions of RTE [19–23]. For the validation of the programs used in this work, MC results were compared with exact analytical relationships [24] obtained for different scattering orders in a nonabsorbing infinite medium geometry. Comparisons showed excellent agreement: for all the scattering functions, the discrepancies used were within one standard deviation of the MC results (the relative discrepancy between MC and analytical results was as small as 0.01%), even when a large number of trajectories (10^8) were simulated. This result guarantees the statistical correctness of the core of the MC codes employed to generate the results presented in Figs. 2–5. The results discussed in this work suggest a further test that can be used for the validation of an MC code: one can compare the results obtained by implementing the four MC methods inside a single code and expect to find a match to within statistical errors. Eventually, with several cross validations and testing we could provide useful numerical phantoms for calculations in tissue optics.

APPENDIX A

The probability density for the variable l_a in the ASPR method is

$$p(l_a) = \mu_a(l_a) \exp\left(-\int_0^{la} \mu_a(\xi)\mathrm{d}\xi\right). \tag{A1}$$

The probability that $l_a > l_i$ is given by

$$P(l_a > l_i) = \int_{li}^{\infty} p(l_a)\mathrm{d}l_a. \tag{A2}$$

By using Eq. (A1), we obtain

$$P(l_a > l_i) = \int_{li}^{\infty} \mu_a(l_a) \exp\left(-\int_0^{la} \mu_a(\xi)\mathrm{d}\xi\right)\mathrm{d}l_a. \tag{A3}$$

We define a new variable y:

$$y(l_a) = \int_0^{la} \mu_a(\xi)\mathrm{d}\xi, \tag{A4}$$

having the differential $dy = \mu_a(l_a)dl_a$. Therefore,

$$P(l_a > l_i) = \int_{\int_0^{li}\mu a(\xi)\mathrm{d}\xi}^{\infty} \exp(-y)\mathrm{d}y = \exp\left(-\int_0^{li} \mu_a(\xi)\mathrm{d}\xi\right). \tag{A5}$$

ACKNOWLEDGMENTS

We wish to thank Prof. Giovanni Zaccanti of the University of Florence for providing useful and fundamental support for

carrying out the Monte Carlo simulations and for several fruitful discussions. We also thank Prof. Irving Bigio and Katherine Calabro of Boston University for useful discussions. This work is supported by National Institutes of Health grant nos. R01 CA154774 and R03-MH093846.

REFERENCES

1. B. C. Wilson and G. Adam, "A Monte Carlo model for the absorption and flux distributions of light in tissue," Med. Phys. **10**, 824–830 (1983).
2. L. Wang, S. L. Jacques, and L. Zheng, "MCML—Monte Carlo modeling of light transport in multi-layered tissues," Comput. Meth. Prog. Biol. **47**, 131–146 (1995).
3. S. T. Flock, M. S. Patterson, B. C. Wilson, and D. R. Wyman, "Monte-Carlo modeling of light-propagation in highly scattering tissues: 1. model predictions and comparison with diffusion theory," IEEE Trans. Biomed. Eng. **36**, 1162–1168 (1989).
4. R. Graaff, M. H. Koelink, F. F. M. Demul, W. G. Zijlstra, A. C. M. Dassel, and J. G. Aarnoudse, "Condensed Monte Carlo simulations for the description of light transport," Appl. Opt. **32**, 426–434 (1993).
5. G. Zaccanti, "Monte Carlo study of light propagation in optically thick media: point source case," Appl. Opt. **30**, 2031–2041 (1991).
6. A. Sassaroli, C. Blumetti, F. Martelli, L. Alianelli, D. Contini, A. Ismaelli, and G. Zaccanti, "Monte Carlo procedure for investigating light propagation and imaging of highly scattering media," Appl. Opt. **37**, 7392–7400 (1998).
7. A. Liebert, H. Wabnitz, N. Zołek, and R. Macdonald, "Monte Carlo algorithm for efficient simulation of time resolved fluorescence in layered turbid media," Opt. Express **16**, 13188–13202 (2008).
8. D. Boas, J. Culver, J. Stott, and A. Dunn, "Three dimensional Monte Carlo code for photon migration through complex heterogeneous media including the adult human head," Opt. Express **10**, 159–170 (2002), http://www.opticsinfobase.org/oe/abstract.cfm?URI=oe-10-3-159.
9. J. M. Schmitt and K. Ben-Letaief, "Efficient Monte Carlo simulation of confocal microscopy in biological tissue," J. Opt. Soc. Am. A **13**, 952–960 (1996).
10. G. Yao and L. V. Wang, "Monte Carlo simulation of an optical coherence tomography signal in homogeneous turbid media," Phys. Med. Biol. **44**, 2307–2320 (1999).
11. B. Farina, S. Saponaro, E. Pignoli, S. Tomatis, and R. Marchesini, "Monte Carlo simulation of light fluence in tissue in a cylindrical diffusing fibre geometry," Phys. Med. Biol. **44**, 1–11 (1999).
12. H. W. Jentink, F. F. M. de Mul, R. G. A. M. Hermsen, R. Graaff, and J. Greve, "Monte Carlo simulations of laser Doppler blood flow measurements in tissue," Appl. Opt. **29**, 2371–2381 (1990).
13. J. L. Reuss and D. Siker, "The pulse in reflectance pulse oximetry: modeling and experimental studies," J. Clin. Monitor. Comput. **18**, 289–299 (2004).
14. F. Martelli, S. Del Bianco, A. Ismaelli, and G. Zaccanti, *Light Propagation through Biological Tissue and Other Diffusive Media: Theory, Solutions, and Software*, Vol. PM193 of SPIE Press Monograph (SPIE, 2009).
15. E. Alerstam, S. Andersson-Engels, and T. Svensson, "White Monte Carlo for time-resolved photon migration," J. Biomed. Opt. **13**, 041304 (2008).
16. E. Alerstam, "Optical spectroscopy of turbid media: time-domain measurements and accelerated Monte Carlo modeling," Ph.D. dissertation (Lund University, 2011).
17. K. W. Calabro and I. Bigio, "On the validity of assumptions to incorporate absorption in Monte Carlo simulations," in *Proceedings of Biomedical Optics*, OSA Technical Digest (Optical Society of America, 2012), paper BSu5A.3.
18. J. J. Duderstadt and W. R. Martin, *Transport Theory* (Wiley, 1979).
19. J. C. J. Paasschens, "Solution of the time-dependent Boltzmann equation," Phys. Rev. E **56**, 1135–1141 (1997).
20. A. Liemert and A. Kienle, "Analytical solution of the radiative transfer equation for the infinite-space fluence," Phys. Rev. A **83**, 015804 (2011).
21. A. Liemert and A. Kienle, "Analytical Green's function of the radiative transfer radiance for the infinite medium," Phys. Rev. E **83**, 036605 (2011).
22. E. Vitkin, V. Turzhitsky, L. Qiu, L. Guo, I. Itzkan, E. B. Hanlon, and L. T. Perelman, "Photon diffusion near the point-of-entry in anisotropically scattering turbid media," Nat. Commun. **2**, 587 (2011).
23. A. Liemert and A. Kienle, "Light transport in three-dimensional semi-infinite scattering media," J. Opt. Soc. Am. A **29**, 1475–1481 (2012).
24. G. Zaccanti, E. Battistelli, P. Bruscaglioni, and Q. N. Wei, "Analytic relationships for the statistical moments of scattering point coordinates for photon migration in a scattering medium," Pure Appl. Opt. **3**, 897–905 (1994).

140.112.174.28 {ts '2020-06-17 10:41:13'}